Evaluation of Unambiguous Vector Winds from the Seasat Scatterometer

DUDLEY B. CHELTON*, MICHAEL H. FREILICH** AND JERRY R. JOHNSON†

*College of Oceanography, Oregon State University, Corvallis, Oregon
**Jet Propulsion Laboratory, California Institute of Technology, Pasadena, California

(Manuscript received 23 February 1989, in final form 19 May 1989)

ABSTRACT

Ambiguity in wind direction has long been an impediment to applications of wind observations from the Seasat scatterometer (SASS). Three months of unambiguous global SASS vector winds (7 July–10 October 1978) have recently become available from the Goddard Space Flight Center (GSFC) Laboratory for Atmospheric Sciences. The directional ambiguities were removed objectively through the use of an atmospheric general circulation model. Elimination of the directional ambiguities greatly enhances the utility of the SASS wind observations. Atmospheric and oceanographic applications of the GSFC vector wind data are given in two companion papers.

The GSFC SASS vector wind dataset has potential utility for many applications, so it is useful to assess the data quality. In this paper, the GSFC data are compared with 14 days of SASS vector winds from the Jet Propulsion Laboratory for which the directional ambiguities were subjectively removed by trained meteorologists using pattern recognition techniques. Both methods are shown to be statistically very similar over the 14-day period. The two methods chose the same solution about 73% of the time and nearest-neighbor solutions about 20% of the time. Reasons for discrepancies are examined and it is concluded that the methods tend to disagree most often in regions of low wind speed and/or highly variable wind direction. The directional differences are generally small and random so that there are no significant differences between spatially and temporally averaged wind fields constructed from the two datasets.

1. Introduction

The Seasat-A Satellite Scatterometer (SASS) measured near-surface winds over the global ocean from 7 July through 10 October 1978. Since that time, there have been few applications of these satellite-measured winds. In part, this is because the relatively short duration of the Seasat mission restricts the range of geophysical problems that can be addressed using the SASS data. A second, and perhaps more restricting limitation has been the ambiguity in wind direction inferred from the SASS data. The dependence of radar backscatter on wind direction relative to antenna pointing angle results in two to four solutions for wind direction when combining measurements from two orthogonal antennas (see section 2). The wind speeds associated with these multiple wind direction solutions are nearly the same. Thus, SASS retrieval of a wind speed is much more straightforward than retrieval of a unique wind direction. Unfortunately, wind speed alone is not sufficient for many geophysical applications, and consequently, SASS data have not received the scientific attention that they might have if the ambiguities in wind direction were removed.

Recently, two important new SASS unambiguous vector wind datasets have emerged. Using two very different methodologies, investigators at the Jet Propulsion Laboratory (JPL) and at the Goddard Space Flight Center (GSFC) Laboratory for Atmospheric Sciences removed the directional ambiguities to produce SASS datasets with a unique wind direction for each observation. The JPL method is based on subjective analysis by trained meteorologists and has been applied to only 14 days of SASS data in September 1978. The GSFC method removes the directional ambiguities objectively using a 6-hour forecast General Circulation Model (GCM) and has been applied to the entire 96 days of SASS data.

It is difficult to make quantitative estimates of the accuracy of either of the datasets. The coverage and spatial resolution of SASS wind measurements far exceed those of any other available wind data. It could be argued that the JPL data are more reliable since the multiple solution vector winds have been scrutinized by trained meteorologists to select a unique "correct" wind direction; however, the JPL wind directions were subjectively chosen to be consistent with the analysts'

† Deceased.

Corresponding author address: Dr. Dudley B. Chelton, College of Oceanography, Oregon State University, Oceanography Admin. Bldg. 104, Corvallis, Oregon 97331-5503.

preconceived notions about the spatial structure and temporal evolution of surface winds. These prejudices are based on years of experience with relatively coarse spatial resolution wind fields constructed from conventional observations and model forecasts. Since SASS wind measurements resolve finer spatial scales than conventional wind measurements, it is possible that the JPL subjective analysis implicitly degrades the quality potentially attainable from SASS winds. On the other hand, the GSFC objective analysis almost certainly degrades the resolution of the SASS winds through explicit use of the finite resolution GSFC atmospheric model (see section 3) to select the "correct" directional ambiguity. It is therefore not obvious whether JPL or GSFC vector wind data are more correct. All other considerations aside, the GSFC dataset is potentially the more useful of the two, since it spans a longer period of time.

The objective of this study is to compare the vector winds produced by the JPL and GSFC ambiguity removal methods for the 14 days of overlap and check for any systematic differences. This comparison draws attention to some possible sources of error in each dataset and provides a first-order evaluation of the quality of the two ambiguity removal techniques. The two datasets are shown to be very similar in a statistical sense. Either dataset could therefore be used to study the spatial structure of global wind fields. The advantages of the GSFC dataset are obvious: the 96-day time span resolves time scales of variability that are of interest to a much broader range of oceanographic and meteorological applications than the 14-day JPL dataset.

In section 2 we briefly review the SASS measurement technique and initial data processing to draw attention to the reason for directional ambiguity in SASS wind observations. Section 3 describes in some detail the JPL and GSFC ambiguity removal methodologies. Quantitative comparisons of the two unambiguous vector wind datasets over the 14-day overlap period are presented in section 4. Descriptive analysis of monthly averaged wind stress and wind stress curl fields constructed from the 96-day GSFC dataset are presented in a companion paper, Chelton et al. (1990). Also included in the companion paper are comparisons of monthly average SASS wind stress fields with NMC model and climatological average estimates of near-surface wind stress and estimates of the global Sverdrup circulation computed from SASS wind stress curl fields. A second companion paper, in preparation, examines in detail global fields of vector winds, wind directional steadiness, divergence, and vorticity, with particular emphasis on the tropical regions.

2. SASS data

Numerous summaries of SASS estimates of near surface winds have been written. A recent review can be found in Freilich and Chelton (1986). Briefly, the characteristics of SASS measurements of radar backscatter depend on the incidence angle, defined to be the angle (measured in the vertical plane) between the incident radiation and the local normal to the sea surface. For incidence angles ranging from about 20° to 60°, radar backscatter is dependent on both wind speed and wind direction. The physics of this relation are not fully understood. It has been shown empirically that, for a given wind direction relative to the antenna pointing angle, backscattered power is related to wind speed by a simple power law (Guinard et al. 1971; Jones and Schroeder 1978). For a fixed wind speed, the backscattered power varies nearly harmonically with wind direction relative to antenna pointing angle (Jones et al. 1977). The backscatter is maximum when the antenna is pointed upward or downwind and minimum when the antenna is pointed crosswind. There is a small asymmetry between the upwind and downwind backscatter. The quantitative relation between backscattered power and wind velocity varies with the incidence angle and the polarization of the transmitted and received radiation.

The underlying harmonic relation between backscatter and wind direction allows the determination of both wind speed and direction when the backscatter from a given region on the sea surface is measured from two or more antenna pointing angles. For Seasat, backscatter measurements were made from a pair of orthogonal antennas on each side of the spacecraft, oriented 45° and 135° relative to the satellite ground track. Forward antenna measurements were combined with nearly collocated aft antenna measurements obtained 1–4 minutes later (depending on incidence angle) to retrieve wind speed and direction. With the Seasat two-antenna configuration, the retrieval results in one to four solutions for the vector winds. The multiple solutions all have nearly the same speed, but may differ widely in direction. For SASS, there were only 15 single-solution cases during the 96-day dataset. Approximately 6% of all SASS wind measurements had two solutions, 11% yielded three solutions, and the remaining 83% had four solutions.

It is worth noting that wind directional ambiguity will not be nearly as much of a problem for the next-generation European Space Agency (ESA) and NASA scatterometers. Both the ESA ERS-1 C-band scatterometer (to be launched in late 1990) and the K_u-band NASA scatterometer (NSCAT, to be launched in 1995 aboard the Japanese ADEOS satellite) will measure radar backscatter from three separate antenna pointing angles. The addition of the third pointing angle measurement should generally result in only two wind solutions, separated by approximately 180°. It is believed that wind direction ambiguity removal (see section 3) will be greatly simplified with this antenna configuration since streamlines of the wind field could be immediately produced.

The multiple-solution SASS wind data used in this study were processed by the Atmospheric Environment Service (AES) of Canada (Baker et al. 1984) using raw data provided by JPL. Measurements of backscatter were binned into 100 km squares. Multiple solution vector winds were retrieved by treating all backscatter measurements within a single square as collocated and using the SASS-I geophysical model function and the SOS wind retrieval algorithm (Schroeder et al. 1982; Boggs 1982). Since this processing, Wentz et al. (1984), Chelton and McCabe (1985) and Woiceshyn et al. (1986) have identified a number of small but statistically significant random and systematic errors in the resulting SASS winds. These errors include a general overestimate of about 1 m s^{-1} in wind speed, an artificial cross-track gradient in wind speed, a substantial overestimation of low wind speeds, and unnecessary data gaps for areas with very low wind speeds. In addition, there are statistical inconsistencies between the winds computed from horizontally and vertically polarized radar observations.

Much less analysis time has been devoted to assessing the accuracies of the wind directions. Wentz et al. (1984) show, however, that the directional dependence of backscatter in the SASS-I model does not agree with measurements obtained from aircraft. Further, Anderson et al. (1987) and others have noted that the distribution of ambiguous direction solutions depends both on the satellite orientation and on the incidence angle. Specifically, a disproportionate fraction of ambiguous vectors point parallel to the scatterometer antenna beam (particularly at high incidence angles). In these cases, wind directions inferred from SASS data may be more closely related to the satellite orientation (relative to north) than to the true wind direction.

Additionally, the sampling characteristics of SASS result in errors in spatial and temporal averages from unresolved short space and time scale variability. Vector winds with approximately 100 km resolution are measured across two 500 km swaths, one on each side of the spacecraft, separated by a 450 km gap centered on the satellite ground track. Successive orbits are separated by about 100 minutes in time and the outer edges of the swaths from successive orbits are separated by about 1200 km at the equator and swaths overlap poleward of about 50° latitude. When wind measurements from both ascending and descending satellite orbits are included, the time-variable winds at a particular location are sampled intermittently by a scatterometer. This sporadic sampling has important repercussions for spatially and temporally averaged SASS winds. It limits the accuracy that can be obtained for wind fields constructed from SASS data. The effects of these sampling errors are briefly examined in section 4c. The essential result based on realistic simulated winds is that the effects of sampling errors are small in monthly averages such as those examined in Atlas et al. (1987) and Chelton et al. (1989).

The numerous measurement errors known to exist in the AES SASS data as summarized above are also likely to have a small effect in monthly average wind fields. Most of the measurement errors are less than 1 m s^{-1} and random. The effects of random errors are greatly reduced since many individual wind observations over a wide range of incidence angles and wind speeds and both horizontally and vertically polarized measurements are included in each spatial and temporal average. Systematic errors are clearly not reduced in these averages. At present, the most significant systematic error known to exist in the AES SASS dataset is the 1 m s^{-1} overestimate of wind speed. We applied a 1 m s^{-1} correction to the SASS data in this study to remove this simple bias. This ad hoc correction is defensible on the basis of independent estimates by Wentz et al. (1984) and Chelton and McCabe (1985). In addition, postexperiment calibration in the JASIN experiment revealed that the "standard" wind recorder overestimated wind speeds by about 10%, corresponding to a 1 m s^{-1} error for the 10 m s^{-1} winds typically observed in JASIN (Weller et al. 1983). The final SASS wind speed algorithm was heavily tuned to the JASIN data, which may at least partly explain the 1 m s^{-1} bias in SASS winds.

3. SASS wind direction ambiguity removal

The methods used by JPL and GSFC to remove the directional ambiguity discussed in section 2 and obtain a unique vector wind for each SASS wind retrieval are summarized in this section. The basis of the JPL scheme is described by Wurtele et al. (1982) and Baker et al. (1984). Under the direction of P. Woiceshyn, teams of investigators at JPL, the University of California at Los Angeles, and AES Canada collaborated to produce a unique vector wind data set for the 14-day period 7–20 September 1978. The first step in ambiguity removal was the generation of near-synoptic plots of AES multiple solution wind vectors covering an entire ocean basin. Such coverage required use of data from multiple, consecutive orbits of the satellite. In all cases, the data used in a single plot were acquired within a 12-hour period. Two teams of analysts, each working independently, constructed streamline analyses of surface winds from the multiple solution wind vector plots using subjective pattern-recognition techniques and all available conventional meteorological measurements, routine weather service forecasts and analyses, and additional data such as satellite cloud photos.

Based on the streamline analyses, regions were identified within the SASS swaths where the subjectively determined wind direction fell within a single quadrant (with axes defined by the instantaneous antenna illumination pattern). Polygons defining these regions were constructed and the vertices of the polygons were digitized for subsequent computer analysis. For each multiple wind solution inside the polygon, the vector

with direction closest to the (nearly constant) direction indicated by the streamline analysis was objectively selected by computer. In this way, each analyst team produced a dataset containing unique vector winds. For much of the data thus processed, the results from the two independent teams were compared. In regions where the two analyses differed, the streamline analysis was repeated until a "consensus" dataset was produced in an iterative fashion.

The GSFC ambiguity removal scheme is described in Atlas et al. (1987). This method also used the AES multiple solution SASS wind vectors. A three-pass iterative procedure to remove the directional ambiguity was applied at 6-hour time steps for the full 96 days of SASS data. At each 6-hour analysis time, vector winds from the GSFC Laboratory for Atmospheric Sciences fourth-order General Circulation Model (GCM) (Kalnay et al. 1983) with 4° latitude by 5° longitude resolution were bilinearly interpolated from the four nearest model grid points to the location of each SASS wind measurement within ±3 hours of the analysis time. The SASS vector wind solution closest to the interpolated model vector wind was chosen to be the "correct" SASS wind if it satisfied specific closeness criteria (see below). These SASS winds, together with available conventional winds for the 6-hour analysis period, were then used to improve the model prediction using a successive correction method (Baker et al. 1984).

In the first pass through the SASS data, the 6-hour model forecast integrated from the previous objective analysis was used as a first guess of the true vector wind field. All one- and two-solution cases of SASS winds within ±3 hours of the analysis time were compared with model winds interpolated to the SASS measurement location. Single solution cases (only 15 over the full 96-day dataset) were accepted as "correct" if they were within 165° of the first-guess direction. For the two-solution cases (6% of the AES SASS data), the solution nearest the first guess was selected if it differed from the first guess by less than 75°; otherwise the SASS wind solution was rejected in the first pass. This set of unique SASS vector winds, along with in situ wind observations for the same 6-hour analysis time, was used to correct the first guess wind field. The resulting surface wind analysis was then used as a first guess of the true vector wind field for the second pass through the SASS data.

In the second pass, all three- and four-solution SASS wind observations (11% and 83%, respectively, of the AES SASS data) within ±3 hours of the analysis time were compared with the first guess winds interpolated to the SASS measurement location. The solution nearest the interpolated first guess was chosen if: 1) it differed from the first guess by less than 30°, and 2) the angle between the nearest solution and the next nearest solution was less than 75°. The set of unique SASS vector winds from the first and second passes, along with available in situ wind observations, were reanalyzed using the successive correction method. The resulting surface wind analysis was then used as a first guess for the third pass through the SASS data.

The third pass considered all remaining one-, two-, three- and four-solution cases of SASS winds within ±3 hours of the analysis time. The solution closest to the interpolated first-guess wind was selected if it differed from the first guess by less than 75°. If none of the multiple solutions for a particular observation were within 75° of the interpolated first guess wind, no unique vector was chosen and the SASS observation was flagged.

All of the resulting unambiguous SASS vector winds and the in situ wind observations were used to correct the surface wind analysis. This final surface wind analysis was integrated forward in time to obtain the first guess vector wind field for the next 6-hour analysis period. The iterative procedure was then repeated to remove the directional ambiguity of all SASS wind measurements within ±3 hours of this next analysis period.

4. Comparison of JPL and GSFC vector winds

As noted previously, neither the JPL nor the GSFC vector winds can be considered "correct." One hopes that any differences between the two datasets are small, as major discrepancies would cast doubt on the value of either dataset. On the other hand, if the two datasets produced by very different techniques are found generally to agree, we can hope that both represent the true vector wind field over the 14-day overlap period. It could then be argued that the GSFC winds are representative of the true vector wind field over the full 96-day dataset. Note, however, that the two methods could also agree and both be wrong. It is difficult to test this possibility since existing high quality in situ datasets are probably inadequate for such a calibration.

In this section, we examine in detail the JPL and GSFC unambiguous vector winds over the 14-day overlap period (7–20 September 1978) for which both datasets exist. The cases where a SASS observation was processed by one scheme but not by the other (referred to here as "mismatches") are discussed in section 4a. The SASS observations processed by both schemes are examined in section 4b. Finally, spatially and temporally averaged JPL and GSFC winds are compared in section 4c.

a. JPL and GSFC mismatches

Over the 14-day overlap period, totals of 380 269 and 304 460 unambiguous winds were produced by JPL and GSFC, respectively, in the latitude range 60°N to 60°S. There were 298 242 observations common to both datasets and 3043 observations were not processed by either method. The primary reason for mismatches becomes apparent from Fig. 1, which shows the locations of the mismatched JPL and GSFC solutions for a representative day (13 September 1978) in the 14-

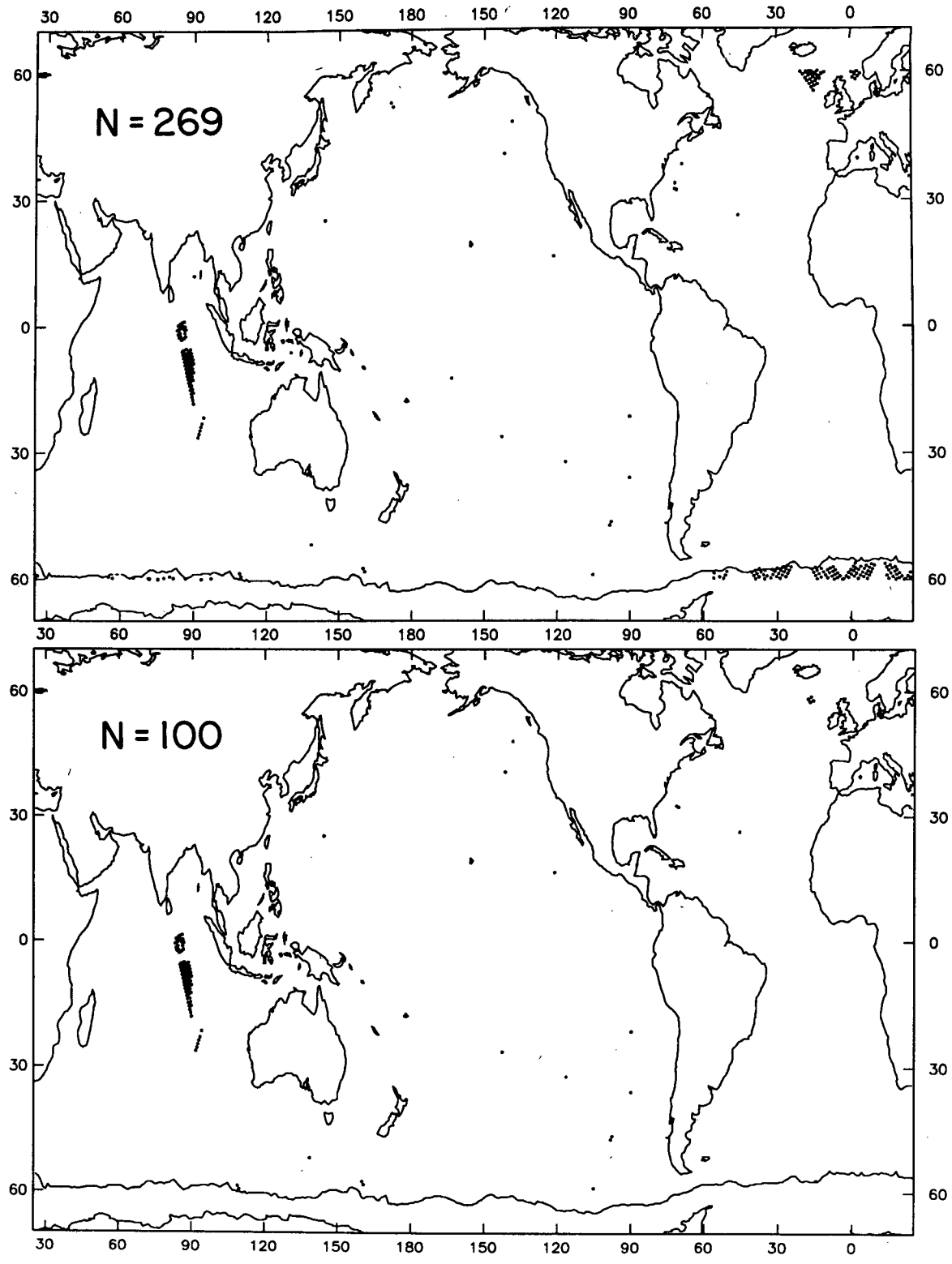

FIG. 1a. Locations of the SASS wind solutions for a typical 24-hour period (this case is 13 September 1978) that were not processed by the JPL ambiguity removal scheme. Each dot corresponds to a missing SASS solution. Upper panel shows all JPL missing solutions between 60°N and 60°S for this day and lower panel shows the missing solutions after eliminating cases over the Antarctic ice sheet and within 500 km of land. The number of missing solutions for this 24-hour period is labeled on each plot. The maximum northward extent of the Antarctic ice sheet during the 96-day Seasat mission is indicated on each plot.

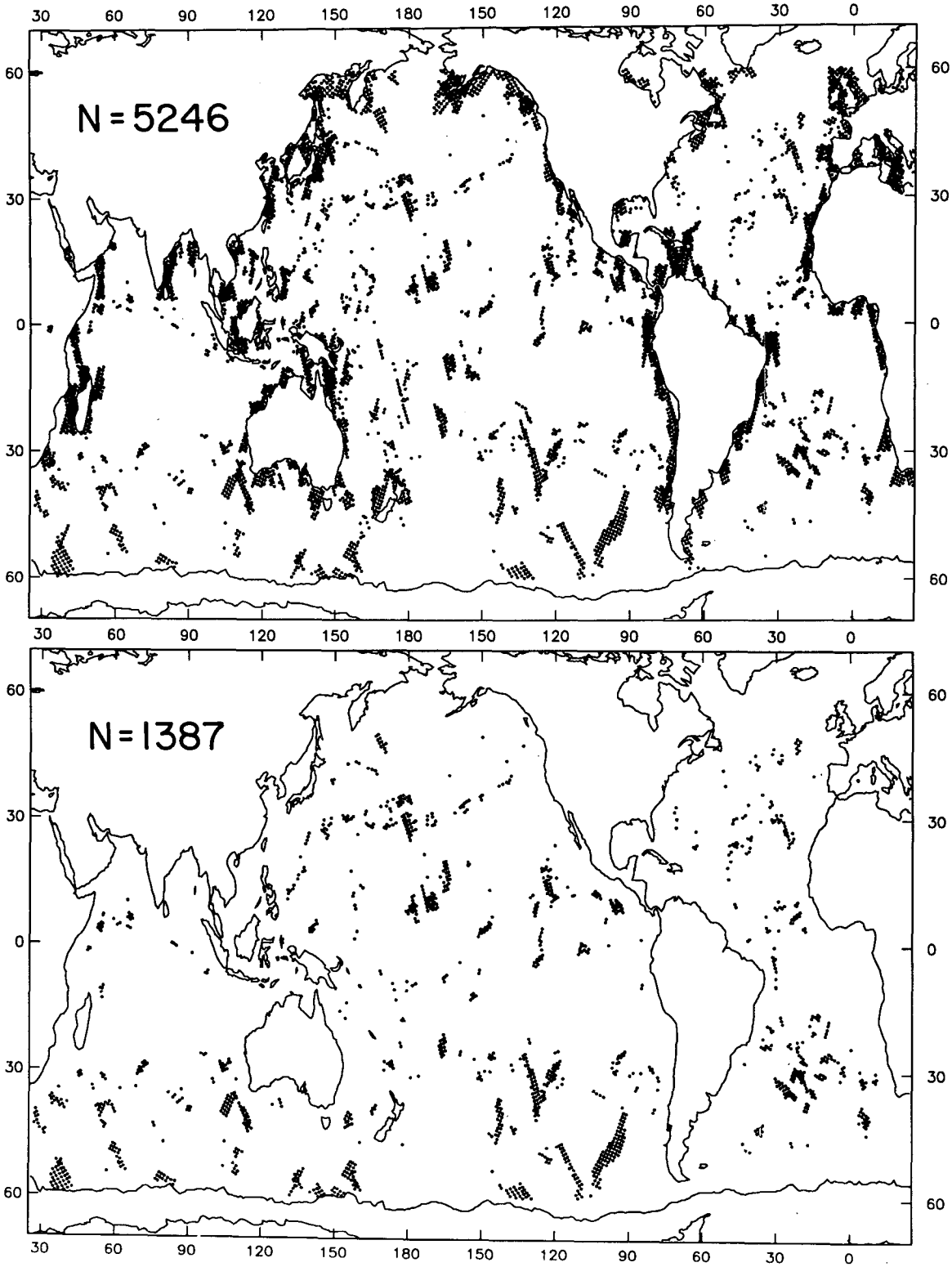

FIG. 1b. As in Fig. 1a, except for the case of the SASS solutions not processed by the GSFC ambiguity removal scheme on 13 September 1978.

day overlap period. For the latitude range 60°N to 60°S in this example, there were 269 SASS observations not processed by the JPL ambiguity removal scheme and 5246 SASS observations not processed by the GSFC ambiguity removal scheme.

A large fraction of the SASS observations not processed by JPL (Fig. 1a) lie poleward of the Antarctic ice boundary as determined from the Seasat scanning multichannel microwave radiometer (Johnson 1986). The JPL scheme used this information about the ice boundary and made no attempt to remove the directional ambiguity of SASS observations over ice since scatterometry can measure near-surface winds only over open water. Over the full 14-day dataset, about half of the missing JPL observations were over the Antarctic ice sheet. The GSFC scheme did not use information about the Antarctic ice boundary and thus attempted to find solutions for the bogus SASS observations over ice. The remaining SASS observations not processed by JPL are generally individual observations randomly scattered around the world oceans, with occasional short segments of an orbit excluded. These correspond to SASS observations which did not fall within any of the polygons defined subjectively by the JPL streamline analyses (see section 3).

The number of SASS observations not processed by GSFC was considerably greater (Fig. 1b). These missing SASS observations are located throughout the oceans, but tend to be concentrated near continental boundaries. This can be explained by the procedure used in the GSFC scheme, which did not remove the directional ambiguity of a SASS observation if any of the four surrounding GCM grid points were located over land. Because of the coarse 4° latitude by 5° longitude resolution of the model, many SASS measurements close to land were not processed by the scheme. Even after accounting for the measurements not processed by GSFC because of their proximity to land, many open-ocean mismatches (Fig. 1b) still evidently did not pass the closeness criteria in the three-step iterative ambiguity removal scheme (see section 3). These SASS observations are randomly located but are apparently quite common.

Of the 389 710 observations available between 60°N and 60°S over the full 14-day overlap period, 6515 were not processed by JPL and 73 706 were not processed by GSFC. As in the example day shown in Fig. 1, the vast majority of these mismatches are either over the Antarctic ice sheet or close to land. If all SASS observations over ice and within 500 km of land are eliminated, the numbers of observations not processed by the two methods are reduced to 3391 and 19 833, respectively.

The latitudinal distributions of the mismatches, both before and after elimination of cases over ice and near land, are shown in Fig. 2b. From this figure it is apparent that, after eliminating the mismatches over ice and near land, the observations not processed by JPL

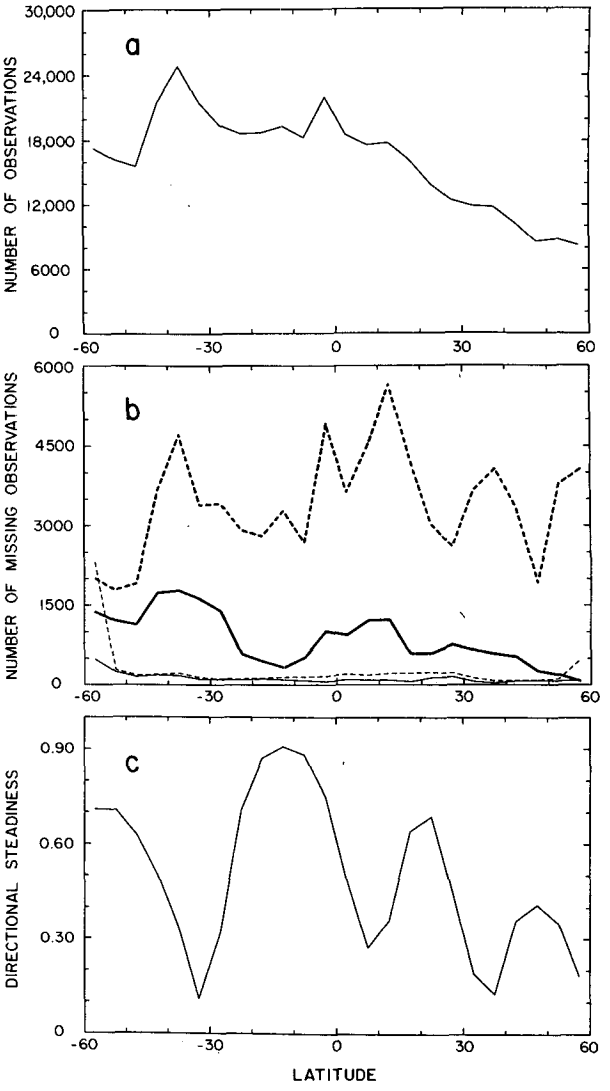

FIG. 2. Latitudinal distributions (stratified by 5° bands) of (a) the total number of SASS solutions for the 14-day overlap period of the GSFC and JPL unambiguous datasets; (b) the numbers of SASS wind solutions not processed by JPL (thin lines) and GSFC (heavy lines) for the 14-day overlap period; dashed lines correspond to total numbers of discrepancies and solid lines correspond to numbers of discrepancies after elimination of cases over the Antarctic ice sheet and within 500 km of land; and (c) the directional steadiness of the winds, defined to be the ratio of the magnitude of vector averaged GSFC winds to the scalar average GSFC wind speed over the 14-day overlap period.

are approximately evenly distributed with latitude. There is, however, some latitudinal dependence of the observations not processed by GSFC. This distribution roughly follows that of the total number of SASS observations (greatest near 40°S, decreasing both northward and southward). A noteworthy exception is the latitude band from about 5° to 25°S where the number of SASS observations not processed by GSFC is disproportionately small compared with the total number

of observations. This improved performance of the GSFC scheme is probably due to the high directional steadiness in this region (see Fig. 2c). (The directional steadiness ranges from a value of 1 for perfectly steady winds to a value of 0 for highly variable wind direction over the 14-day period.) Because of the relatively uniform direction of the southeast tradewinds, it is likely that the GCM directional forecast skill is high in this region. Then, assuming that one of the SASS multiple solutions is the true vector wind (or at least close to it), it would not be surprising to find fewer cases where none of the multiple SASS solutions were close to the model winds.

It is constructive to examine the wind speeds associated with the mismatches. The average wind speeds over the 14-day overlap period computed from the SASS observations processed by one of the ambiguity removal methods but not by the other are plotted by 5° latitudinal bands in Fig. 3. The somewhat noisier appearance of the curve for the cases processed only by GSFC (dashed line) is not surprising in view of the relatively small number of such cases. However, the latitudinal distribution of the wind speeds of these mismatches is approximately the same as the overall average wind speed computed from the SASS observations processed by both JPL and GSFC (heavy continuous line). The interesting feature in Fig. 3 is that the average wind speeds of the SASS observations processed only by JPL (thin continuous line) are consistently lower than the overall average wind speed by 0.5–1.5 m s^{-1}. Evidently the GSFC ambiguity removal scheme encounters more cases where none of the multiple SASS solutions fall close to the model prediction when the wind speeds are small, and therefore rejects the observation.

This discrimination against low wind speeds is not presently understood. One possible explanation is that the GCM used by the GSFC scheme produced relatively less reliable wind directions in regions of light winds where dynamical constraints are weak and the physical constraints that take over are not well understood. Then if one of the multiple SASS solutions was nearly correct, there would be a higher probability that the model wind direction differed from all of the SASS solutions by more than the maximum separation allowed by the ambiguity removal scheme. An alternative explanation is that the SASS vector wind solutions may be less reliable in regions of light winds and would thus be rejected more often because none of the multiple solutions satisfy the closeness criteria of the GSFC scheme. Quite likely, both effects contribute to the preferential GSFC rejection of low wind speeds.

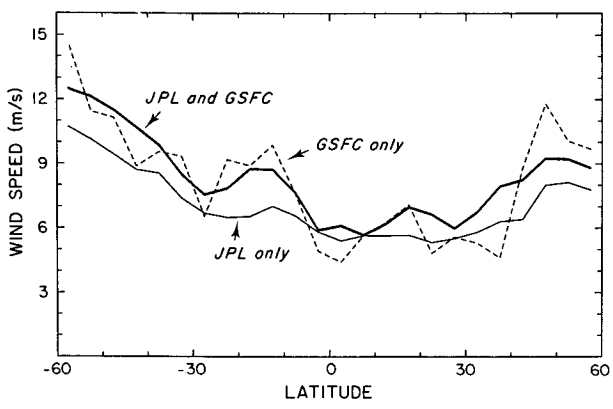

FIG. 3. Latitudinal distribution (by 5° bins) of the average wind speeds of the SASS solutions processed only by GSFC (dashed line) and processed only by JPL (thin continuous line). Heavy continuous curve corresponds to average wind speed computed from the cases processed by both JPL and GSFC.

In any case, the total number of cases rejected by the GSFC scheme (excluding those within 500 km of land) was less than 10% of the total processed. The impact of the preferential treatment of light winds would therefore be relatively small in the monthly average wind fields examined in Atlas et al. (1987) and Chelton et al. (1990).

b. JPL and GSFC matched observations

The 298 242 SASS observations processed by both the JPL and GSFC schemes are examined in detail in this section in order to quantify the level of agreement between the two methods and to try to understand the causes for any disagreements. The most obvious comparison is to determine the frequency with which the two ambiguity removal schemes selected exactly the same vector solution. An equally important question is: when the two schemes selected different vector solutions, were they nearly the same direction or were they widely separated in direction? Figure 4 illustrates schematically the possible relations between different SASS vector solutions selected by the two methods for two-, three-, and four-solution cases. Two of the solution vectors in a single SASS observation are often separated by only a small angle. If JPL selected one of these solutions and GSFC the other, it would be difficult to judge which was correct. On the other hand, if the two methods selected solution vectors separated by a large angle in a high percentage of cases, this would cast doubt on the reliability of either or both of the ambiguity removal schemes.

The relative number of cases for which the JPL and GSFC methods selected exactly the same solution, nearest neighbor solutions, second nearest neighbor solutions and third nearest neighbor solutions are summarized in Table 1. The statistics are segregated by SASS solution type (two-, three-, and four-solution cases) and by hemisphere. Overall, the two schemes selected exactly the same solution 73% of the time, nearest neighbor solutions 20% of the time and second or third nearest neighbor solutions 5% and 2% of the time, respectively. The fact that either the same or the nearest neighbor solutions were selected 93% of the

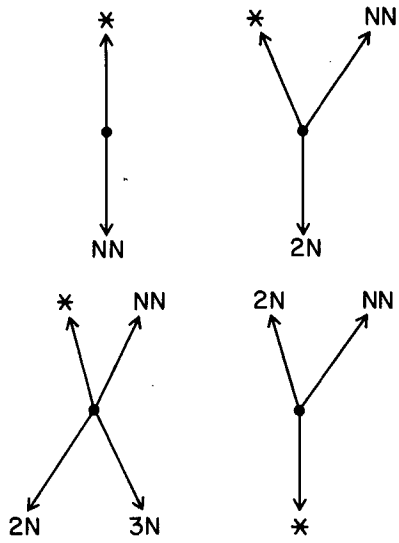

FIG. 4. Schematic diagram illustrating the relation between the SASS solution selected by GSFC (denoted by an asterisk) and the other possible SASS solutions for 2, 3 and 4 solution cases. Nearest-neighbor solutions are denoted by NN, and second- and third-nearest-neighbor solutions are denoted by 2N and 3N, respectively.

time is encouraging and suggests that the overall performances of the two methods are comparable.

For the two solution cases (a total of 16 753 for the 14-day overlap period, generally separated by about 180°), the two ambiguity removal schemes selected the same solution more than 96% of the time. This may have relevance to the future ERS-1 and NSCAT scatterometers. With measurements of radar backscatter from three different antenna pointing angles, ERS-1 and NSCAT winds are expected to have only two possible direction solutions, separated by approximately 180°, in 90% of the cases (compared with only 6% of the cases for SASS). Automated ambiguity removal is likely to be much simpler for ERS-1 and NSCAT than it was for SASS.

Another important conclusion that can be drawn from Table 1 is that, overall, there is no significant difference in the performance of the GSFC objective ambiguity removal technique in the Northern versus the Southern Hemisphere. This result is somewhat surprising since the GSFC technique relies heavily on a GCM to select a unique SASS direction solution (section 3). Since atmospheric GCMs are generally believed to be more reliable in the Northern than in the Southern Hemisphere (Yu and McPherson 1984; Levy et al. 1989), one might expect the GSFC ambiguity removal skill to deteriorate in the Southern Hemisphere. These results may indicate that the iterative assimilation technique in the GSFC algorithm uses the SASS data to update and improve the GCM for the Southern Hemisphere to a quality comparable to that of the Northern Hemisphere, at least for near-surface winds. This would imply a positive impact of scatterometer data assimilation on near-surface analyses from atmospheric models, which may also influence model forecasts.

The statistics presented in Table 1 are useful for formulating a rough comparison of the two SASS unique vector wind datasets. The differences in wind

TABLE 1. Percentages of matched SASS solutions for which the directional ambiguities selected by the JPL and GSFC schemes were exactly the same (SS), nearest-neighbor solutions (NN), second-nearest-neighbor solutions (2N) and third-nearest-neighbor solutions (3N). See Fig. 4 for a schematic summary of these cases. Statistics are broken down by Northern and Southern hemispheres and global ocean.

	Percent total matched solutions	SS	NN	2N	3N
		Global ocean			
All matched cases	100.0	73.1	20.0	5.0	1.9
2 solution cases	6.2	96.4	3.6	—	—
3 solution cases	11.2	74.9	21.5	3.6	—
4 solution cases	82.6	71.1	21.1	5.5	2.3
3 and 4 solution cases	93.8	71.5	21.1	5.3	2.1
		Northern Hemisphere			
All matched cases	100.0	71.8	20.0	5.8	2.5
2 solution cases	4.6	95.2	4.8	—	—
3 solution cases	10.2	74.7	21.1	4.2	—
4 solution cases	85.2	70.2	20.7	6.3	2.9
3 and 4 solution cases	95.4	70.7	20.7	6.0	2.6
		Southern Hemisphere			
All matched cases	100.0	71.8	20.1	4.5	1.6
2 solution cases	7.2	96.9	3.1	—	—
3 solution cases	11.7	75.1	21.6	3.3	—
4 solution cases	81.1	71.6	21.6	5.0	2.0
3 and 4 solution cases	92.8	72.0	21.3	4.8	1.8

direction selected by the two ambiguity removal schemes (GSFC minus JPL) can be examined in greater detail from the histograms in Fig. 5. Direction differences were stratified by 5° bins ranging from −180° to +180°. The relative numbers of observations in each bin are shown for the global ocean and the Northern and Southern hemispheres separately. In these figures, the spike in the bin centered at 0° corresponds to cases where the two methods selected exactly the same solution. The cases where the two methods selected nearest neighbor, second nearest neighbor and third nearest neighbor solutions are indicated by shading in these figures, as described in the figure caption.

The direction differences in cases where the two methods selected different solutions are bimodally distributed with peaks at about ±60°. This is due to the fact that 75% of all cases where the two ambiguity removal schemes differed consisted of nearest neighbor solutions, which are separated by about 20°–80° in direction (see Fig. 5). The angular separations of the second and third nearest neighbor solutions are also evident from Fig. 5 (90°–150° and approximately 180°, respectively). Note that these does not appear to be any significant difference between the distributions for the Northern and Southern hemispheres, nor is there any apparent preference for clockwise or counterclockwise nearest-neighbor solutions. A more detailed examination by 20° latitudinal bands in each ocean (see Johnson 1986) showed small preferences for clockwise or counterclockwise solutions in some regions, but the asymmetry was never more than a few percent and was inconsistent from one region to another.

A geographical summary of the comparison statistics is given in Table 2. The frequency of same solution cases ranged from highs of about 80% in the southeast trade winds (20°S to 0°) of all three ocean basins to a low of 63.3% in the intertropical convergence zone in the Pacific Ocean (0° to 20°N). The asymmetry between agreement in the Northern and Southern Hemisphere tropics was smaller in the Atlantic and Indian Oceans, but still significant. The reduced agreement in the bands from 0° to 20°N is likely due to the low wind speeds and low directional steadiness in the convergence regions between the northeast and southeast trade winds of all three ocean basins. Another noteworthy feature is the lower frequencies of same-solution cases in the westerlies of the South Pacific and South Atlantic oceans (66.6% and 69.6%, respectively, for 60° to 40°S) than in corresponding latitudes of the Northern Hemisphere (76.1% and 80.2%, respectively). These latitude bands coincide with the locations of the polar front and mean storm tracks in each hemisphere. Finally, note the lower agreement in the horse latitudes of the South Indian Ocean (66.8% for 40° to 20°S), where the wind speed and directional steadiness are both low.

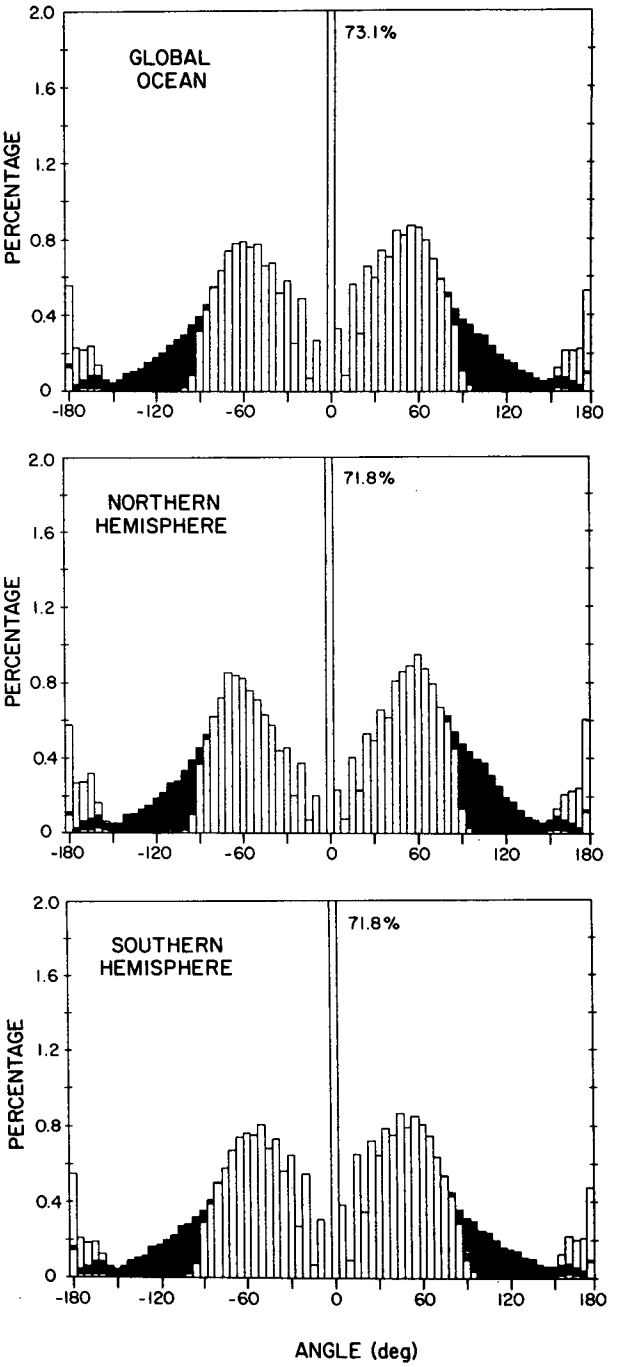

FIG. 5. Histograms of GSFC minus JPL wind direction differences for the global ocean and Northern and Southern hemispheres separately. Direction differences are stratified by 5° bins. The spike centered at 0° corresponds to cases where the two ambiguity removal schemes selected exactly the same solution; the percentage of observations in this bin is labeled on each plot. The white boxes between 0° and approximately 90° correspond to cases where nearest-neighbor solutions were selected by the two schemes. The black boxes between approximately 90° and 180° correspond to second-nearest-neighbor solutions and the white boxes over black boxes correspond to third-nearest-neighbor solutions. The small white boxes under the black boxes near 180° correspond to nearest-neighbor solutions for the two solution cases.

TABLE 2. Statistics of the comparisons between the GSFC and JPL unambiguous data sets over the 14-day overlap period 7–20 September.

Ocean region	Latitude range	Percent exact agreement	Percent within 45°	Percent within 90°	Average angle difference (deg)	Rms. angle difference (deg)
Global ocean	60°S–60°N	73.1	80.1	92.7	−0.61	45.4
Northern Hemisphere	0°–60°N	71.8	77.4	90.7	−1.04	49.1
Southern Hemisphere	60°S–0°	71.8	81.6	93.3	−0.36	43.1
Atlantic Ocean	60°–40°S	69.6	78.2	90.0	0.27	50.7
	40°–20°S	72.2	80.9	93.2	−1.86	42.6
	20°S–0°	81.3	89.2	98.0	−0.61	27.8
	0°–20°N	72.7	78.1	91.8	−1.63	46.3
	20°–40°N	73.8	80.7	94.7	0.48	40.2
	40°–60°N	80.2	86.7	95.7	−1.04	33.9
Indian Ocean	60°–40°S	73.4	83.5	94.5	2.57	38.7
	40°–20°S	66.8	75.1	89.5	−0.12	53.4
	20°S–0°	79.9	89.6	97.4	−2.48	27.8
	0°–20°N	69.9	75.8	91.4	0.75	49.9
Pacific Ocean	60°–40°S	66.6	76.2	90.0	−1.52	51.8
	40°–20°S	71.9	78.9	92.5	−1.18	45.8
	20°S–0°	80.0	86.5	96.1	1.22	33.8
	0°–20°N	63.3	69.4	85.9	−1.98	59.3
	20°–40°N	74.9	80.9	92.3	−0.42	44.9
	40°–60°N	76.1	82.4	92.4	−1.74	44.0

Table 2 also gives other statistics which help to quantify the relation between the JPL and GSFC vector wind solutions. Overall, the average angle differences between the two datasets are small everywhere, supporting the earlier argument that there is no significant asymmetry between clockwise and counterclockwise neighboring solutions. The last column of the table gives the rms angle difference between the two datasets. This statistic should be interpreted with some caution since the direction differences are not normally distributed (Fig. 5). Nonetheless, it is useful as a measure of the overall similarity between the two datasets. Note from Table 2 that the two ambiguity removal schemes selected vector wind solutions within the same quadrant in approximately 93% of the cases; about 80% of the time they selected solutions within the same octant. The relative frequencies varied from these overall averages by as much as 10% in some geographical regions in a manner consistent with the geographical variation of the other statistics in Table 2.

Examination of the dependencies of the direction differences on environmental conditions identifies some important causes for differences in vector wind solutions selected by the two ambiguity removal schemes. A number of possible relationships were investigated, including dependencies of direction differences on day number, 6-hour analysis time of the GCM, local time of day, latitude, longitude, wind speed and wind directional steadiness. No systematic dependencies on time (day number, GCM analysis time or local time) were detected. Dependencies on latitude and longitude were found, but it is believed that these apparent geographical dependencies are mostly a reflection of dependencies on wind speed and wind directional steadiness (Johnson 1986). Thus, only the dependencies on these last two factors are discussed here. The presence of fronts might also result in more frequent discrepancies between the vector solutions selected by the two methods, but these features would be more difficult to quantify from the SASS data alone without detailed case-by-case studies.

The relation between wind speed and the directional agreement between the two ambiguity removal schemes is summarized in Fig. 6. All of the matched SASS solutions were stratified by 0.5 m s^{-1} wind speed bins. The number of observations within each bin is shown in Fig. 6a. The relative number of cases for which JPL and GSFC both selected the same solution are plotted in Fig. 6b. The frequency of agreement increases approximately linearly from 45% at 0.5 m s^{-1} (where the importance of wind direction is rather dubious anyway) to about 80% at 11 m s^{-1}. For higher wind speeds, the frequency of agreement remains approximately constant at about 80%.

This relation between wind speed and directional differences is summarized in another way in Fig. 6c, which shows the average absolute value of the angle differences for each wind speed bin. The ±1 standard deviation error bars on the plot show the 1-standard deviation range of values in each wind speed bin. The average angle difference decreases approximately linearly from about 70° at 0.5 m s^{-1} to about 15° at 11

m s^{-1} and remains constant at about 15° for higher wind speeds. The scatter within each wind speed bin decreases with increasing wind speed (a standard deviation of about 90° at 0.5 m s^{-1}, decreasing to about 40° at 11 m s^{-1}). The noisiness of average angle differences for wind speeds greater than 21 m s^{-1} (also evident in the percentage of same solutions in Fig. 6b) is due to sampling errors from the small number of solutions at these high wind speeds.

From Fig. 6, it is apparent that the two ambiguity removal schemes selected the same direction solution more often when the wind speeds were high. It appears that a wind speed of about 11 m s^{-1} represents a threshold, above which the agreement between the two schemes no longer improves with increasing wind speed. A possible explanation for poorer agreement between the two ambiguity removal schemes in regions of lower wind speed is that the GCM winds become progressively less reliable with decreasing wind speed (i.e., the errors in the GCM wind direction increase). Such behavior would lead to more errors in the SASS vector wind solution selected by the three-pass iterative procedure used by GSFC to remove the wind directional ambiguity.

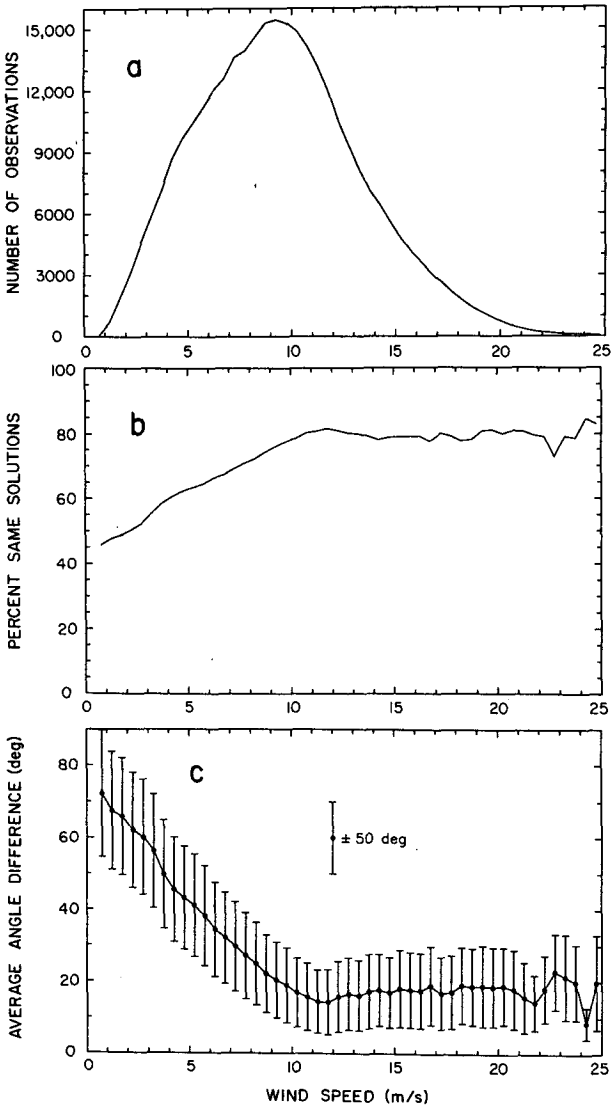

FIG. 6. Distributions as a function of wind speed of (a) total number of observations; (b) percentage of observations for which JPL and GSFC selected the same solution; and (c) average and standard deviation of the absolute value of the angle difference (GSFC minus JPL). Note the different scale for the ±1 standard deviation error bars; the scale for a range of ±50° is shown in the lower panel. In all plots, the wind observations over the 14-day overlap period were stratified by 0.5 m s^{-1} wind speed bins.

The relation between wind directional steadiness and the directional agreement between the two ambiguity removal schemes is summarized in Fig. 7. Directional steadiness is defined to be the ratio of the magnitude of vector averaged winds to the scalar averaged wind speed over the 14-day overlap period. The directional steadiness for regions where the wind direction never changes (but the wind speed may change) is 1; directional steadiness decreases as the wind direction becomes more variable. All of the matched SASS solutions were stratified by directional steadiness bins of 0.05, and the number of observations within each bin is shown in Fig. 7a. Note that the directional steadiness over this 14-day overlap period may be skewed somewhat toward high values because of the short period over which the directional steadiness was computed.

The frequency with which JPL and GSFC both selected the same solution is plotted in Fig. 7b. The values for low directional steadiness are somewhat noisy due to the small number of observations. For directional steadiness greater than 0.25, however, the percentages of agreement gradually but steadily increase from 65% to 85% for steady winds.

The relation between directional steadiness and the average absolute value of the angle difference between GSFC and JPL wind directions is shown in Fig. 7c. The angle differences decrease with increasing directional steadiness. Values range from about 35°–40° for directional steadiness less than 0.5 and decrease progressively to about 5° for steady winds. The scatter within each directional steadiness bin also decreases with increasing directional steadiness, with a remarkably small standard deviation of only 1.7° in the highest directional steadiness bin.

From Fig. 7, a very clear dependence of the directional differences between the two ambiguity removal schemes on wind directional steadiness is apparent. The two methods selected the same direction solution more often in regions of high directional steadiness, i.e., in regions where the winds do not fluctuate greatly in direction. The lower agreement in regions of low directional steadiness may be due to an inability of the GCM to resolve short time scale variations in the wind field, thus introducing errors in the GSFC selection of the SASS vector wind solution.

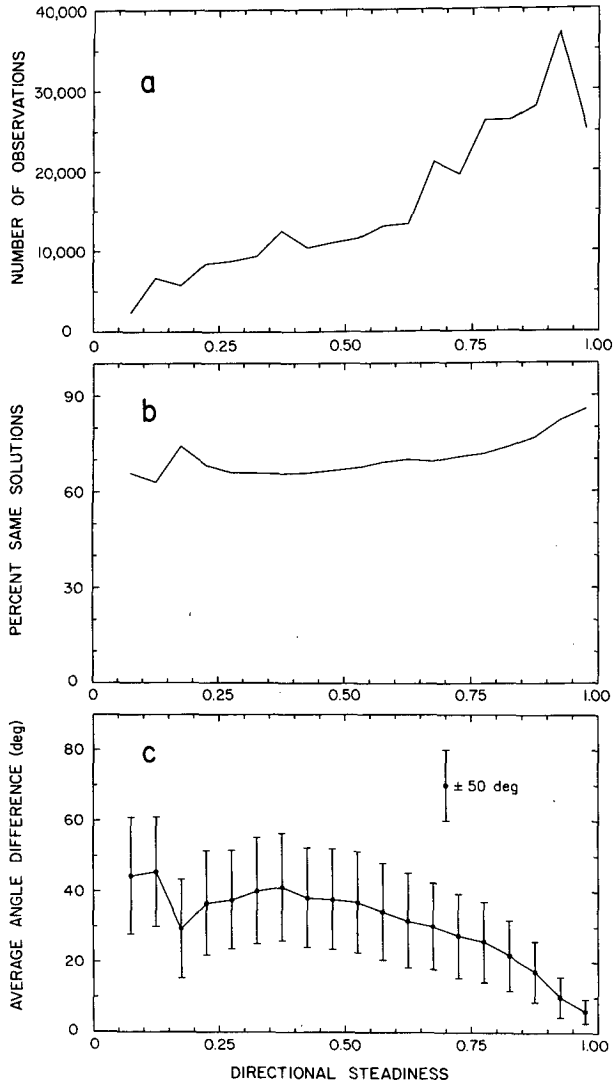

FIG. 7. As in Fig. 6 except distributions as a function of directional steadiness. The wind observations were first stratified globally by 5° latitude–longitude regions and the directional steadiness of the GSFC winds over the 14-day overlap period was computed for each 5° region. The wind observations were then stratified by bin sizes of 0.05 in directional steadiness according to the appropriate value for the 5° region defining the location of the observation.

We conclude from this section that both wind speed and directional steadiness are important factors in determining the expected agreement between the two ambiguity removal schemes. Since these quantities are geographically variable, it is not surprising that the agreement between the two schemes is also geographically dependent, as can be seen from Table 2. From Figs. 6b and 7b, it appears that the upper limit on the percentage of cases for which JPL and GSFC selected the same solution is about 80%. That is, the two methods selected the same solution in, at best, about four out of five cases. The likelihood that the two methods selected the same solution decreases with decreasing wind speed and decreasing directional steadiness. As shown in Table 1 and Fig. 5, however, in about 75% of the cases where the two methods selected different solutions, they picked nearest neighbor SASS solutions typically differing by only about 30°–70°.

c. Spatially and temporally averaged JPL and GSFC winds

The comparisons between individual observations in the 14 days common to both the JPL and GSFC datasets (examined in detail in section 4b) drew attention to the environmental conditions that lead to discrepancies between the two ambiguity removal methods. If the cases where the two vector solutions differ are random, i.e., there is no systematic difference between clockwise and counterclockwise neighboring solutions, then spatially and temporally averaged vector wind fields constructed from the two data sets should be very similar. This is an important question which has bearing on the quality of the monthly averaged wind fields examined in Atlas et al. (1987) and Chelton et al. (1990). The 14-day overlap period (limited by the duration of the JPL dataset) is too short to quantify the agreement between JPL and GSFC winds averaged over monthly time scales. It should also be kept in mind that it is not known whether the 14-day overlap period is representative of the full 96-day SASS dataset. There are a wide variety of meteorological features in this dataset, however, so we have no a priori reason to expect that the period from 7–20 September 1978 is unique. Comparisons between 14-day averaged JPL and GSFC vector winds would therefore provide a useful measure of the agreement between wind fields constructed from the two datasets.

Fourteen-day averaged vector winds were computed globally on a 4° latitude by 10° longitude grid for both the JPL and GSFC datasets. Only the 298 242 SASS solutions for which the directional ambiguity was removed by both schemes were included in the averages. The magnitudes (speeds) and directions of the vector averaged wind speeds for each 4° × 10° region were compared. The differences (GSFC minus JPL) were stratified by bin sizes of 0.5 m s^{-1} in wind speed and 2° in wind direction. There were no significant differences between the Northern and Southern hemispheres (Johnson 1986). The frequencies of observations in each bin for the global ocean are shown in Fig. 8.

While the direction differences between individual JPL and GSFC observations (Fig. 5) were bimodally distributed, the direction differences in these spatial and temporal averages are unimodally distributed (Fig. 8a). The histogram has a very sharp and well-defined peak in the bin centered on 0°, accounting for 15% of the observations. The direction differences in these averages are tightly clustered around 0°, with 75% of the cases between ±10° and 88% of the cases between ±20°.

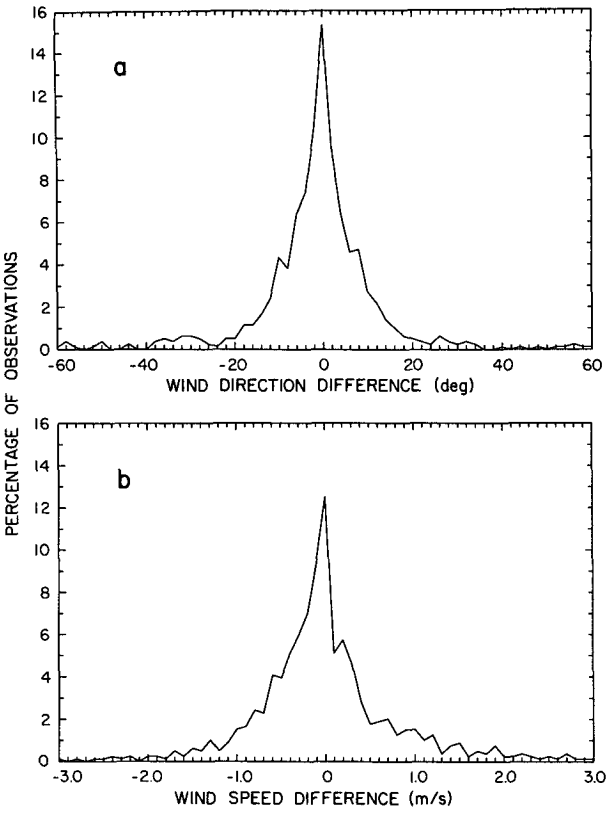

FIG. 8. Histograms of (a) the direction differences and (b) the speed differences between 14-day averaged JPL and GSFC wind fields on a 4° latitude by 10° longitude global grid. Speed and direction differences were stratified by bin sizes of 0.5 m s^{-1} and 2°, respectively.

The wind speed differences in these 14-day, 4° × 10° temporal and spatial averages are also unimodally distributed and tightly clustered around zero (Fig. 8b). The maximum is 13% in the bin centered on 0 m s^{-1}, with 84% of the cases within ±1 m s^{-1} and 96% of the cases within ±2 m s^{-1}.

The close agreement between wind speeds and wind directions in the 14-day, 4° × 10° averages indicates that the individual cases where JPL and GSFC selected different SASS solutions indeed show no preference between clockwise and counterclockwise neighboring solutions. As noted previously in Table 2, about 93% and 80% of the individual observations in the JPL and GSFC datasets were within the same quadrant and octant, respectively. Since the differences in wind direction are random and symmetric about zero, the wind speed and direction differences are small in spatially and temporally averaged vector wind fields. It is concluded that these 14-day averaged wind fields are not highly sensitive to the method used to remove the ambiguity in SASS wind direction.

Although it is not possible to determine the level of agreement between monthly averages of JPL and GSFC vector winds due to the 14-day limitation of the JPL dataset, it is possible to quantify the relative effects of sampling errors alone in 14-day versus monthly averages. As noted previously in section 2, the winds at any particular location are sampled intermittently by the ascending and descending orbits of a satellite scatterometer. For a 2.5° latitude–longitude region, the average number of 100-km footprint SASS samples per day for the 3-day repeat orbit period of the Seasat mission ranged from less than 1 in the tropics, to about 2 at 60° latitude and about 4 at 70° latitude (Fig. 9). The increase with latitude is due to the convergence and overlap of successive ground tracks at high latitudes. (The abrupt decrease at about 67° latitude is due to the northern and southern limits of sampling by the port and starboard SASS swaths, respectively, with the 108° Seasat orbit inclination.) The discrete sampling of a continuously variable wind field results in sampling errors due to aliasing of unresolved high-frequency variability.

The effects of this aliasing on spatially and temporally averaged wind fields constructed from discontinuous scatterometer observations can be quantified from a simple simulation. For the purposes of illustration, it was assumed that the winds are spatially homogeneous over a 2.5° region. The temporal variability over the 2.5° region was specified from spectra of observed (nearly continuous) components of wind speed at three locations: a high-latitude case at Ocean Weather Station P (50°N, 145°W), a middle-latitude case appropriate for 30°N, and a low-latitude case based on measurements at 0°, 150°W. For each case, 100 synthetic time series of duration 100 days were generated with the observed spectral energy but random phases at each frequency. Each synthetic time series was then sampled at the SASS observation times, thus simulating discrete error-free scatterometer measurements of a continuously variable wind field.

Averages of the nearly continuous time series (the "true" averages) and the subsampled time series (the simulated scatterometer averages) of a wind speed

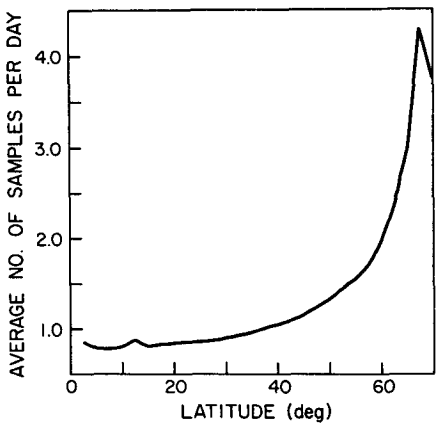

FIG. 9. The average number of SASS samples per day for a 2.5° latitude–longitude region as a function of latitude for the Seasat 3-day repeat orbit.

component were then computed for averaging periods ranging from 3 to 30 days. The root-mean-square (rms) differences between the true averages and the scatterometer averages, ensemble averaged over the 100 synthetic time series and over all existing averaging periods within each 100-day time series, are plotted as a function of averaging period in Fig. 10. Not surprisingly, the rms error decreases with increasing averaging period. The change in rms error is very rapid at short averaging periods and more gradual at longer averaging periods. Roughly speaking, the error curve follows an $N^{-1/2}$ dependence on the number of observations N in the averages, as would be expected from simple consideration of the variance of sample means.

For present purposes, the interest is in the rms error at 14 and 30 day averaging periods. At 14 days, the rms error is about 0.45 m s^{-1} for the equatorial and midlatitude cases and 0.55 m s^{-1} for the high latitude case. The larger rms error at high latitudes is due to more energetic unresolved high-frequency variability. The error is reduced by about 25% (to about 0.33 and 0.39 m s^{-1}, respectively) for 30-day averages. Note that these simulations place a lower bound on the accuracy of temporally averaged wind fields. Incorporating measurement errors in the simulations increases these rms errors only slightly.

The essential conclusion of these simulations is that the level of agreement between monthly averages of JPL and GSFC data (if such long averages were possible with the JPL data) could be expected to be perhaps as much as 25% better than the results obtained for 14-day averages. Moreover, smoothing the 2.5° averages of vector winds to give spatial resolution comparable to the 4° × 10° averages examined in Fig. 8 will reduce the error even more. We therefore feel confident that the monthly averaged GSFC wind fields examined in Atlas et al. (1987) and Chelton et al. (1990) are representative of the true winds over these space and time scales.

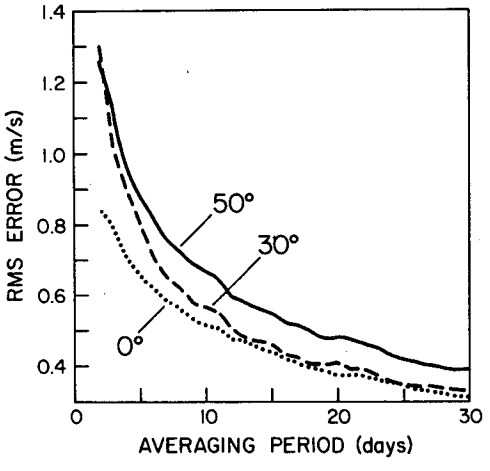

FIG. 10. Root-mean-square difference between true averages and simulated scatterometer averages of a wind speed component over a low, middle, and high latitude 2.5° region.

5. Conclusions

An inherent limitation of scatterometer observations of winds is the inability to determine the wind direction unambiguously (section 2). The radar returns from short gravity–capillary waves on the sea surface yield up to four solutions for the near-surface vector wind. The multiple solutions have nearly the same speed but vary widely in direction. An automated objective scheme (section 3) for removing the directional ambiguity from scatterometer wind solutions has been developed and applied to the complete SASS dataset under the direction of R. Atlas at the Goddard Space Flight Center (GSFC). The GSFC SASS data have been extensively evaluated in this paper as a prelude to examining global ocean surface wind forcing in the companion paper (Chelton et al. 1990).

The quality of the GSFC SASS vector wind solutions was investigated by comparison with 14 days of SASS vector winds for which the directional ambiguity had been subjectively removed using pattern recognition techniques by trained meteorologists under the direction of P. Woiceshyn at the Jet Propulsion Laboratory (JPL). On a case-by-case basis, the GSFC and JPL SASS solutions are statistically similar. The two methods of directional ambiguity removal agreed exactly about three times out of four. It is impossible to say which method is better from the analysis presented here. Reasons for discrepancies between the two methods were examined in section 4b and it was concluded that the two methods tend to disagree most often in regions of low wind speeds and/or highly variable wind direction (low directional steadiness).

For the cases when the two ambiguity removal methods selected different direction solutions, they chose nearest-neighbor SASS vector solutions about 75% of the time. In total, the two methods selected directions within the same octant in about 80% of the cases and within the same quadrant in about 93% of the cases. The differences in directions appear to be random and hence average to near zero in spatial and temporal averages of the vector winds. Averages over 4° of latitude by 10° of longitude and 14 days (the maximum overlap of the GSFC and JPL datasets) were examined in section 4c. About 90% of the gridded averages agree to within ±20° in wind direction and ±1.5 m s^{-1} in wind speed.

Finally, it was shown from simulations in section 4c that wind speed errors in 2.5° latitude–longitude averages are reduced to less than 0.4 m s^{-1} in monthly averages. Smoothing the 2.5° gridded data reduces the error even further. We conclude that a high degree of confidence can be placed in the accuracy of spatially and temporally averaged wind fields constructed from the full three months of GSFC SASS data. The integrity

of the GSFC SASS data is further supported by comparisons with operational meteorological forecast wind field analyses and climatological average winds in the companion papers Chelton et al. (1990) and a paper in preparation; in regions where in situ observations are plentiful, the agreement between SASS and conventional wind fields is very good in monthly averages.

Acknowledgments. We thank Peter Woiceshyn at JPL and Robert Atlas at GSFC for providing the two SASS vector wind datasets used in this analysis and Gad Levy for constructive and helpful comments on the manuscript. We gratefully acknowledge financial support from NASA Grant NAGW-730 and Contract 957580 from the Jet Propulsion Laboratory funded under the NSCAT Announcement of Opportunity.

REFERENCES

Anderson, D., A. Hollingsworth, S. Uppala and P. Woiceshyn, 1987: A study of the feasibility of using sea and wind information from the ERS-1 satellite. Part I. Wind scatterometer data. European Space Agency Contract Rep., 121 pp.

Atlas, R., A. J. Busalacchi, M. Ghil, S. Bloom and E. Kalnay, 1987: Global surface wind and flux fields from model assimilation of Seasat data. *J. Geophys. Res.*, **92,** 6477–6487.

Baker, W. E., R. Atlas, E. Kalnay, M. Halem, P. M. Woiceshyn, S. Peteherych and D. Edelmann, 1984: Large-scale analysis and forecast experiments with wind data from the Seasat-A scatterometer. *J. Geophys. Res.*, **89,** 4927–4936.

Boggs, D. H., 1982: The Seasat scatterometer model function: the genesis of SASS-I. Rep. 622-230. Jet Propul. Lab., Pasadena, Calif., 30 pp.

Chelton, D. B., and P. J. McCabe, 1985: A review of satellite altimeter measurement of sea surface wind speed: with a proposed new algorithm. *J. Geophys. Res.*, **90,** 4707–4720.

——, A. M. Mestas-Nunez and M. H. Freilich, 1990: Global wind stress, wind stress curl and Sverdrup circulation from the Seasat scatterometer. *J. Phys. Oceanogr.*, in press.

Freilich, M. H., and D. B. Chelton, 1986: Wavenumber spectra of Pacific winds measured by the Seasat scatterometer. *J. Phys. Oceanogr.*, **16,** 741–757.

Guinard, N. W., J. T. Ransone and J. C. Daley, 1971: Variation of the NRCS of the sea with increasing roughness. *J. Geophys. Res.*, **76,** 1525–1538.

Johnson, J. R., 1986: Analysis of Seasat-A satellite scatterometer wind observations with emphasis over the Antarctic Circumpolar Current. M.S. thesis, Oregon State University, 260 pp. [Available from: D. B. Chelton, College of Oceanography, Oceanography Admin. Bldg. 104, Oregon State University, Corvallis, OR 97331-5503.]

Jones, W. L., and L. C. Schroeder, 1978: Radar backscatter from the ocean: Dependence on surface friction velocity. *Bound-Layer Meteor.*, **13,** 133–149.

——, L. C. Schroeder and J. L. Mitchell, 1977: Aircraft measurements of the microwave scattering signature of the ocean. *IEEE Trans. Antennas Propag.*, **1,** 52–61.

Kalnay, E., R. Balgovind, W. Chao, D. Edelmann, J. Pfaendtner, L. Takacs and K. Takano, 1983: Documentation of the GLAS Fourth Order General Circulation Model. NASA Tech. Memo 86064.

Levy, G., R. A. Brown and D. B. Chelton, 1989: Southern Hemisphere synoptic mean sea level pressure from space. *Quart. J. Roy. Meteor. Soc.*, submitted.

Schroeder, L. C., D. H. Boggs, G. Dome, I. M. Halberstam, W. L. Jones, W. J. Pierson and F. J. Wentz, 1982: The relationship between wind vector and normalized radar cross section used to derive Seasat-A satellite scatterometer winds. *J. Geophys. Res.*, **87,** 3318–3336.

Weller, R. A., R. E. Payne, W. G. Large and W. Zenk, 1983: Wind measurements from an array of oceanographic moorings and from F/S Meteor during JASIN 1978. *J. Geophys. Res.*, **88,** 9689–9705.

Wentz, F. J., S. Peteherych and L. A. Thomas, 1984: A model function for ocean radar cross sections at 14.6 GHz. *J. Geophys. Res.*, **89,** 3689–3704.

Woiceshyn, P. M., M. G. Wurtele, D. H. Boggs, L. F. McGoldrick and S. Peteherych, 1986: The necessity for a new parameterization of an empirical model for wind/ocean scatterometry. *J. Geophys. Res.*, **91,** 2273–2288.

Wurtele, M. G., P. M. Woiceshyn, S. Peteherych, M. Borowski and W. S. Appleby, 1982: Wind direction alias removal studies of Seasat scatterometer derived wind fields. *J. Geophys. Res.*, **87,** 3365–3377.

Yu, T. W., and R. D. McPherson, 1984: Global data assimilation experiments with scatterometer winds from Seasat-A. *Mon. Wea. Rev.*, **112,** 368–376.